Expert Systems with Applications 38 (2011) 12107–12115

Contents lists available at ScienceDirect

Expert Systems with Applications

journal homepage: www.elsevier.com/locate/eswa

# A novel neural network with simple learning algorithm for islanding phenomenon detection of photovoltaic systems

Kuei-Hsiang Chao [a,*], Chia-Lung Chiu [a], Ching-Ju Li [a], Yu-Choung Chang [b]

[a] Department of Electrical Engineering, National Chin-Yi University of Technology, Taiwan
[b] Green Energy & Environment Research Laboratories, Industrial Technology Research Institute, Taiwan

ARTICLE INFO

*Keywords:*
Intelligent islanding phenomenon detection
Photovoltaic (PV) power generation system
Extension distance
Extension theory
Extension neural network (ENN)

ABSTRACT

This study aimed to propose an intelligent islanding phenomenon detection method for a photovoltaic power generation system. First, a PSIM software package was employed to establish a simulation environment of a grid-connected photovoltaic (PV) power generation system. A 516W PV array system formed by Kyocera KC40T photovoltaic modules was used to complete the simulation of the islanding phenomenon detection method. The proposed islanding phenomenon detection technology was based on an extension neural network (ENN), which combined the extension distance of extension theory, as well as the learning, recalling, generalization and parallel computing characteristics of a neural network (NN). The proposed extension neural network was used to distinguish whether the trouble signals at the grid power end were power quality interference or actual islanding operations, in order that the islanding phenomenon detection system could cut off the load correctly and promptly when a real islanding operation occurs. Finally, the feasibility of the proposed intelligent islanding detection technology was verified through simulation results.



## 1. Introduction

When a photovoltaic power generation system is connected with a grid power system to supply power, and the grid power is cut off due to a malfunction, the photovoltaic power generation system cannot detect the problem and cut the power. This situation results in an independent power supply phenomenon, which is called an islanding operation. Once an islanding operation occurs, a protective device should immediately detect and stop it; otherwise there may be a negative impact on the power supply system or power users (Task, 2002). When an islanding operation occurs, if the gap between the total output power of a photovoltaic power generation system and the total consumed power of the load in the area of the islanding operation exceeds a certain degree, then, the voltage and frequency of the system would change significantly. At this moment, over/under voltage relay (OVR/UVR) and over/under frequency relay (OFR/UFR) can be used for detection to avoid the continuation of the islanding operation; however, when the output and load consumption of a photovoltaic power generation system approach a balance, the changes in voltage and frequency of the system are not sufficient for detection by the voltage and frequency relays; this is called the non-detection zone of relay in this paper (Mango, Liserre, & Aquila, 2006a; Mango, Liserre, & Aquila, 2006b). Therefore, other methods must be used for detection of an islanding operation in order to avoid the phenomenon continuing.

At present, the existing islanding operation detection methods can be divided into passive (IEEE Std. 1547, 2003; Jeraputra & Enjeti, 2004; Jones, Sims, & Imece, 1990; Mango et al., 2006a, 2006b) and active detection modes (Hung, Chang, & Chen, 2003; John, Ye, & Kolwalkar, 2004; Ye, Kolwalkar, Zhang, Du, & Walling, 2004; Ye et al., 2004). The passive detection technique monitors the load end states, such as voltage, frequency, and phase angle to judge whether there is an islanding operation. The passive detection technique mainly includes a voltage phase jump detection method, a frequency change rate detection method, and the third harmonic distortion of a voltage surge detection method (Mango et al., 2006a, 2006b). However, only the third harmonic distortion of a voltage surge detection method lacks a non-detection zone, the other two detection methods have non-detection zones, the size of the non-detection zone depends on the sensitivity of the relay. The non-detection zone is large if the sensitivity of the relay is low, however, the non-detection zone can be reduced if the sensitivity of relay is increased, but a misoperation is likely to occur as a result, which influences the stability of the relay. The sensitivity of the relay should not be set too high, in consideration of the stability of the relay, thus, it is necessary to use an active detection mode together with a passive detection mode in order to remedy the deficiency.

* Corresponding author. Tel.: +886 4 2392 4505x7272; fax: +886 4 2392 2156.
*E-mail address:* chaokh@ncut.edu.tw (K.-H. Chao).

0957-4174/$ - see front matter © 2011 Elsevier Ltd. All rights reserved.
doi:10.1016/j.eswa.2011.02.175

During ordinary operations, the active detection mode initiatively exerts a periodic disturbance on the voltage or frequency of the system in parallel operation mode. Since the grid power system is a very stable reference supply, the disturbance of the active detection mode does not exert a significant influence on the system voltage or frequency under normal conditions. However, when an islanding operation occurs, the system loses its stable reference power supply, and this disturbance to the active detection mode would cause instability in the system. Even if the power generation output and load consumption are balanced, the disturbance would break the balanced state of power, and the obvious voltage or frequency changes of the system at this point would cause the islanding operation to be detected. The active detection method mainly includes an active voltage drift method, an active frequency drift method, a slip mode frequency shift method, and a load variation method (Ye, Kolwalkar, et al., 2004; Ye, Li, et al., 2004). However, the power system may experience an electrical disturbance from an external force, which would be regarded as an islanding detection. Therefore, this paper adopts an extension neural network (ENN) based multi-variable method that combines passive and active detection modes to detect an islanding operation, where the photovoltaic power generation system can be promptly cut from load when the grid power becomes disconnected, furthermore, it can distinguish whether the trouble signal at the grid end is derived from a power quality disturbance or an actual islanding operation.

## 2. The proposed extension neural network (ENN)

The extension neural network theory combines the concept of an extension theory with the concept of a neural network, and calculates the relations among various data through the extension distance (ED). Fig. 1 shows the architecture of an extension neural network; it has input and output layer neurons, the input data are first classified in the architecture, and are then read in the extension neural network, the output layer stores the calculated extension distance. The connection between the input layer and the output layer is the weighting factor, which includes the upper limit of the weighting factor, the weighting center, and the lower limit of the weighting factor. Finally the minimum ED value of the output layer of different types is determined, and the type of data is judged (Chao, Li, & Wang, 2009; Wang, 2003).

### 2.1. Learning process of extension neural network

The extension neural network is of supervised learning, which means first inputting a characteristic sample, if the characteristic sample does not match the preset target value, then, the weighting factor shall be modified, and the accuracy rate of the identification system can be effectively improved by adjusting the weighting factor.

The parameters are defined before learning, first the learning sample is defined by $X = \{X_1, X_2, X_3, \ldots X_{N_p}\}$ and $N_p$ is the total amount of the learning samples, each sample contains the characteristic and type of data $X_i^p = \{x_{i1}^p, x_{i2}^p, x_{i3}^p, \ldots, x_{in}^p\}$, among which $i = 1, 2, 3, \ldots, N_p$, and $n$ is the characteristic number, and $p$ is the type. If $N_m$ is the total number of errors, then, the total error ratio, $E_\tau$ can be defined as follows:

$$E_\tau = \frac{N_m}{N_p} \tag{1}$$

The learning rule of an extension neural network is described as follows (Chao et al., 2009; Wang, 2003):

*Step 1:* Set up extension matter-element model, and set the weighting factor between input and output layers, the $k$th matter-element model can be expressed as

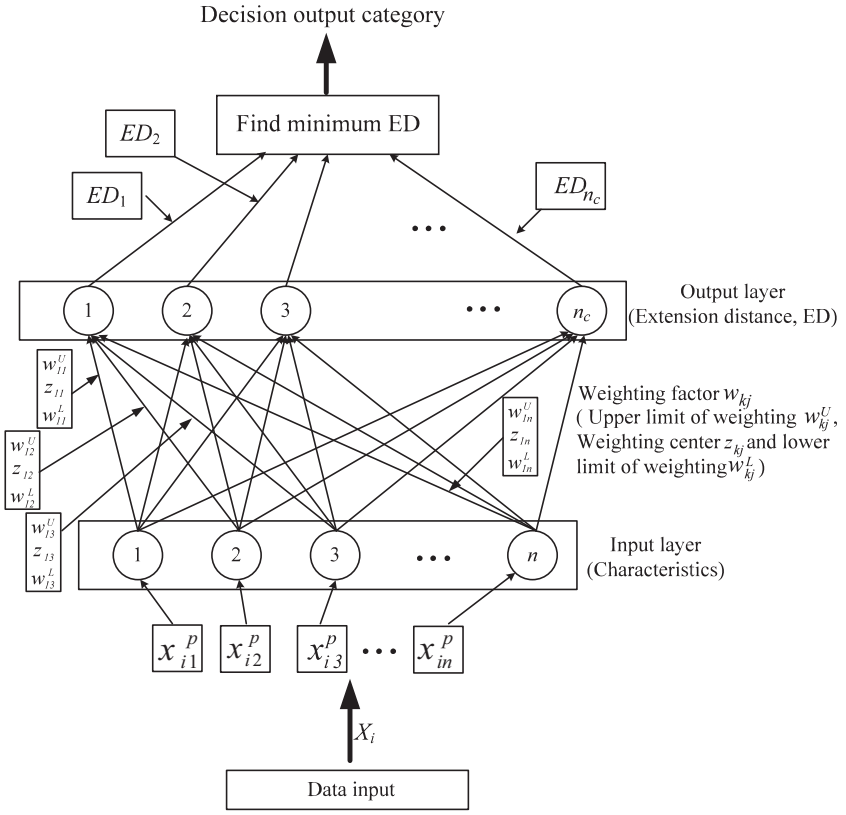


**Fig. 1.** Extension neural network architecture diagram.

$$R_k = \begin{bmatrix} N_k, & c_1, & V_{k1} \\ & c_2, & V_{k2} \\ & c_j, & V_{kj} \end{bmatrix} \quad j = 1,2,\ldots,n;\ k = 1,2,\ldots,n_c \tag{2}$$

$N_k$: the name of the $k$th type.
$c_j$: the $j$th characteristic of $N_k$.
$V_{kj}$: the classical region $\langle w^L_{kj}, w^U_{kj}\rangle$.
$n_c$: total classification clusters of output end.
The classical regions $w^U_{kj}$ and $w^L_{kj}$ of ENN are:

$$w^L_{kj} = \min_{i\in N_p}\{x^p_{ij}\} \tag{3}$$

$$w^U_{kj} = \max_{i\in N_p}\{x^p_{ij}\} \tag{4}$$

where, $x^p_{ij}$ represents the learning data of ENN at input end.

*Step 2:* Find the weighting center $z_{kj}$ of each cluster.

$$\mathrm{Z}_k = \{\mathrm{z}_{k1}, z_{k2}, \ldots, z_{kn}\} \tag{5}$$

$$\mathrm{z}_{kj} = \frac{(w^U_{kj} + w^L_{kj})}{2} \tag{6}$$

Among which $j = 1, 2, \ldots, n$; $k = 1, 2, \ldots, n_c$

*Step 3:* Read in the $i$th learning sample of $p$ type, expressed as

$$X^p_i = \{x^p_{i1}, x^p_{i2}, \ldots, x^p_{in}\}, x \in n_c \tag{7}$$

*Step 4:* Use (8), the extension distance equation to calculate the distance between learning sample and various clusters.

$$ED_{ik} = \sum_{j=1}^{n}\left[\frac{|x^p_{ij} - z_{kj}| - (w^U_{kj} - w^L_{kj})/2}{|(w^U_{kj} - w^L_{kj})/2|} + 1\right], \quad k = 1,2,\ldots,n_c \tag{8}$$

where, $x^p_{ij}$ is the $i$th learning sample of type $p$, and the characteristic of type $p$ is $j$; $z_{kj}$ is the weighting factor center of $j$th input end point and $k$th output end point.

*Step 5:* The new cluster $k^*$ can be obtained after the calculation of extension distance, and $ED_{ik^*} = \min\{ED_{ik}\}$. If $k^* = p$, skip to step 7 directly; on the contrary, execute step 6.

*Step 6:* Adjust and update the weighting factors of $p$th and $k^*$th clusters as follows:

(1) Update the weighting center values of $p$th and $k^*$th clusters.

$$z^{new}_{pj} = z^{old}_{pj} + \eta(x^p_{ij} - z^{old}_{pj}) \tag{9}$$

$$z^{new}_{k^*j} = z^{new}_{k^*j} - \eta(x^p_{ij} - z^{new}_{k^*j}) \tag{10}$$

(2) Update the weighting factors of $p$th and $k^*$th clusters.

$$\begin{cases} w^{L(new)}_{pj} = w^{L(old)}_{pj} + \eta(x^p_{ij} - z^{old}_{pj}) \\ w^{U(new)}_{pj} = w^{U(old)}_{pj} + \eta(x^p_{ij} - z^{old}_{pj}) \end{cases} \tag{11}$$

$$\begin{cases} w_{k^*j^{L(new)}} = w^{L(old)}_{k^*j} + \eta(x^p_{ij} - z^{old}_{k^*j}) \\ w^{U(new)}_{k^*j} = w^{U(old)}_{k^*j} + \eta(x^p_{ij} - z^{old}_{k^*j}) \end{cases} \tag{12}$$

$\eta$: the learning rate of extension neural network.
$z^{new}_{pj}$: the new weighting center value of characteristic $j$ of type $p$ after learning.
$z^{old}_{pj}$: the old weighting center value of characteristic $j$ of type $p$ before learning.
$z^{new}_{k^*j}$: the new weighting center value of characteristic $j$ of cluster $k^*$ after learning.
$z^{old}_{k^*j}$: the old weighting center value of characteristic $j$ of cluster $k^*$before learning.
$w^{L(new)}_{pj}$: the new lower limit of weighting of characteristic $j$ of type $p$.
$w^{U(new)}_{pj}$: the new upper limit of weighting of characteristic $j$ of type $p$.
$w^{L(old)}_{pj}$: the old lower limit of weighting of characteristic $j$ of type $p$.
$w^{U(old)}_{pj}$: the old upper limit of weighting of characteristic $j$ of type $p$.
$w^{L(new)}_{k^*j}$: the new lower limit of weighting of characteristic $j$ of cluster $k^*$.
$w^{U(new)}_{k^*j}$: the new upper limit of weighting of characteristic $j$ of cluster $k^*$.
$w^{L(old)}_{k^*j}$: the old lower limit of weighting of characteristic $j$ of cluster $k^*$.
$w^{U(old)}_{k^*j}$: the old upper limit of weighting of characteristic $j$ of cluster $k^*$.

*Step 7:* This learning is finished after all the samples are classified, otherwise, repeat the calculation procedure from Step 3 to Step 6.

*Step 8:* When the total error rate $E_\tau$ meets the expected target value, stop the calculation procedure, otherwise, return to Step 3 to continue.

Fig. 2 shows the adjustment process of the weighting factors, as described in step 6. The learning sample $x_{ij}$, in Fig. 2(a), belongs to cluster $B$. However, the result of the extension distance equation is $ED_A < ED_B$, thus, it is classified as cluster $A$. As shown in Fig. 2(b), after the adjustment of the weighting factor, the new extension distance is $ED'_A > ED'_B$, hence, the learning sample $x_{ij}$ can be classified as cluster $B$.

### 2.2. Calculation procedure of extension neural network

Once the learning process is completed, identification or classification can be conducted, the calculation procedure is:

*Step 1:* Read in weighting matrix of ENN
*Step 2:* Read the sample to be identified
*Step 3:* Use (8) to determine the extension distance value between the identification sample and the cluster after learning
*Step 4:* Determine the minimum extension distance to judge what cluster type the identification sample is
*Step 5:* Check whether all samples are detected, stop calculation if the identification is finished, otherwise return to step 2 and read the new sample to be identified.

## 3. Extension neural network based islanding detection method

This paper uses an extension neural network with passive and active multi-variable detection methods for the detection of islanding operations. Fig. 3 shows the architecture diagram of the intelligent islanding operation detection system, which contains a power conditioner, an LC-filter, an intelligent islanding phenomenon detection controller, a grid power, and a load. Among which, $V_{dc}$ is the DC voltage of the output for the photovoltaic module array through the converter. The peak voltage of the power conditioner, the frequency of output voltage of the power conditioner, and the phase difference between the voltage and current of the power conditioner can be calculated through the voltage and current feedback signals, and the obtained signals can be used as the index of islanding detection.

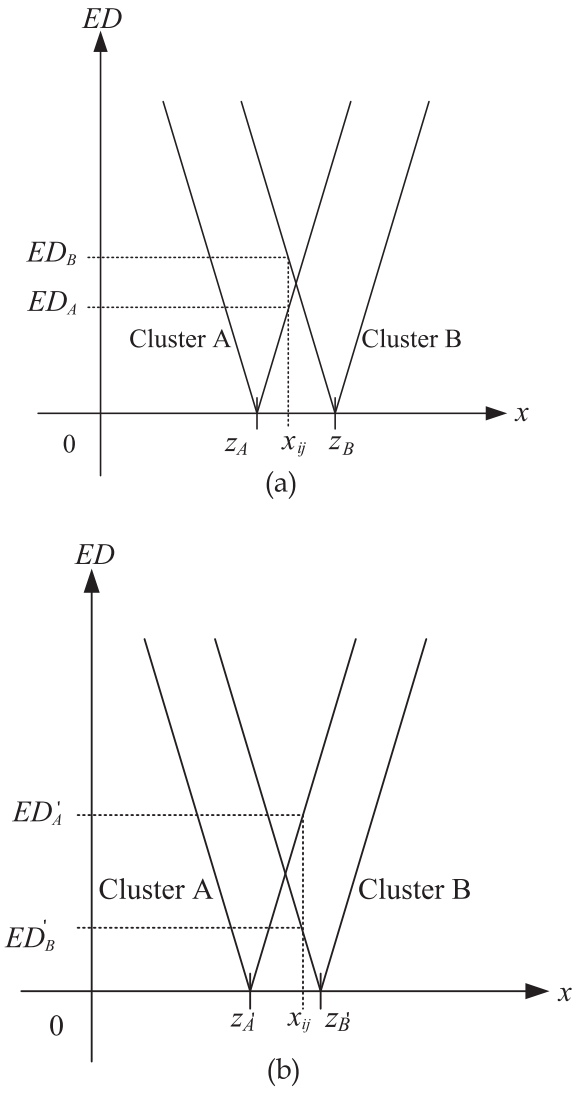


**Fig. 2.** Adjustment process of cluster weighting: (a) before adjustment; (b) after adjustment.

### 3.1. Construction of matter-element models

This paper simulates the situation of a disconnected grid power with a RLC parallel load as shown in Fig. 3, where the extension neural network islanding operation characteristics are selected as:

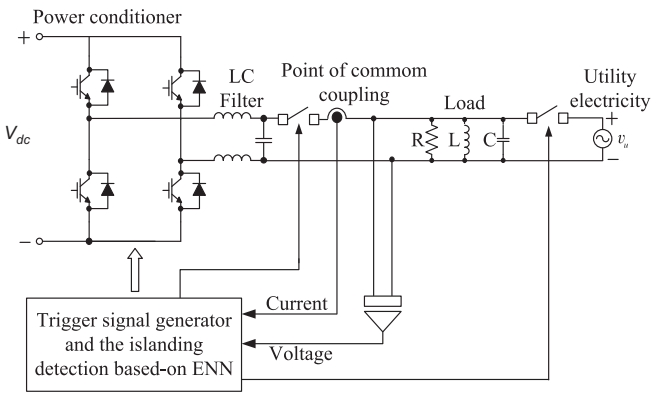


**Fig. 3.** Architecture diagram of the intelligent islanding phenomenon detection system.

1. *Peak voltage*: the maximum output voltage value of the power conditioner.
2. *Frequency*: the frequency of output voltage of the power conditioner.
3. *Phase difference*: the phase difference between output voltage and current of the power conditioner.

Therefore, the matter-element model of islanding phenomenon detection technology in this paper is defined as:

$$R_k = \begin{bmatrix} N_k, & c_1, & V_{k1} \\ & c_2, & V_{k2} \\ & c_3, & V_{k3} \end{bmatrix} \tag{13}$$

where, $N_k$ denotes the islanding phenomenon detection type, $c_1$ and $c_2$ denote the peak voltage and frequency of output of the power conditioner, respectively, $c_3$ denotes the phase difference between output voltage and current of the power conditioner, and $V_{k1} \sim V_{k3}$ are the range values of the three characteristics, respectively (i.e. classical region).

Power systems may suffer from lightning, salt damage, collision with foreign objects, or violent variations in load, which could result in a voltage swell, voltage dip, voltage flicker, or power harmonic within the system, hence, may be interpreted as an islanding detection by the system. Therefore, this paper uses an extension neural network for the detection of islanding operations through different environments of power quality in order to identify power quality disturbances or islanding operations within a photovoltaic power generation system; hereinafter, all the factors influencing the power quality are discussed (IEEE Std. 1159-1995, 1995; Taiwan Power Company. Power Quality).

(1) *Voltage swell*: as defined by IEEE Std. 1159-1995, the root-mean-square value of the grid voltage is between 1.1 p.u.(per unit) and 1.8 p.u., for the duration of a 0.5 period.
(2) *Voltage dip*: as defined by IEEE Std. 1159-1995, a voltage dip refers to the root-mean-square value of a grid voltage is 0.1 p.u. ∼ 0.9 p.u., and the duration is 0.5 period to 1 minute.
(3) *Power harmonic*: voltage harmonic means the grid power system contains a third, fifth, or seventh harmonic component, and various harmonics defined in this paper are 10%, 7%, and 5% of fundamental frequency, respectively.
(4) *Voltage flicker*: the simulated voltage flicker in this paper is derived from combining a low frequency voltage source (15 Hz and 20 Hz) with the standard voltage of 60 Hz.

There are seven types of operational phenomena in this paper, according to the system's voltage swell, voltage dip, injected with power harmonic, normal operation, islanding operation above normal operating limit, islanding operation below normal operating limit, and voltage flicker. In addition, 360 data obtained in seven operating states are divided into 235 learning data and 125 identification data. The islanding detection matter-element model, as shown in Table 1, can be obtained by calculating the 125 learning data according to the learning process of the extension neural network, as shown in Section 2.1, and the preset parameters of the learning process of the extension neural network as follows:

(1) *Learning rate*: 0.001
(2) *Learning times*: 200 times
(3) *Characteristic number*: 3
(4) *Type number*: 7
(5) *Fault tolerance rate*: 0 (i.e. learning accuracy must reach 100%).

### 3.2. Identification procedure

The upper and lower limits of weighting and weighting centers of various characteristic values through the learning process extension neural network are shown in Table 2.

The detection steps of the extension neural network islanding detection method are listed as follows:

*Step 1*: Read in the weighting factors of ENN islanding detection after learning.
*Step 2*: Read 125 identification data samples.
*Step 3*: Use (8) to calculate the extension distance between 125 entered identification data and each cluster.
*Step 4*: Look for the minimum extension distance, which can be determined from the calculated distance in step 3, and judge the type of identification data.
*Step 5*: Check whether all the samples are detected, stop calculation if identification is completed, otherwise return to step 2 to read identification data samples.

Fig. 4 is the flow chart of the extension neural network islanding detection system, as put forward in this paper, first the output voltage and the current of the power conditioner are detected, then, the voltage peak, frequency, and phase difference between voltage and current are calculated, and then the active voltage drift method is adopted to judge whether there is an islanding operation, according to the aforesaid identification process.

## 4. Simulation results

In this paper, Kyocera KC40T (Kyocera Solar Industries) photovoltaic modules are connected as a photovoltaic power generation system with a rated output voltage of 208V (12 modules connected in series), a rated output current of 2.48A, and a rated output power of 516W, through a PSIM simulation software package (Powersim Inc., 2001–2003) to simulate islanding detection. Fig. 5 shows when the output of a power conditioner is connected with the grid power in parallel, the grid power is disconnected from the system at the fourth second, the islanding detection system detects the islanding operation in 0.5 period (about 8.3 ms), and then, cuts off the load. The strip time conforms to the standards for islanding operations, as constituted by (Sandia National Laboratories SAND, 2000-1939), namely the maximum voltage strip period is 1 period (about 16 ms). Fig. 6 shows when the grid power end has an islanding operation occurring at about the fourth second, while the system has experienced three periods of voltage swells, as seen, the ENN islanding detection method can distinguish the voltage swell is from a signal interference from an

**Table 1**
Islanding detection matter-element model after extension neural network learning.

| Category of islanding detection | Matter-element model of islanding detection |
|---|---|
| I1: Voltage swell | $R_1 = \begin{bmatrix} N_1, & c_1, & \langle 277.938, 572.271\rangle \\ & c_2, & \langle 59.1848, 60.4438\rangle \\ & c_3, & \langle -31.6, 19.4\rangle \end{bmatrix}$ |
| I2: Voltage dip | $R_2 = \begin{bmatrix} N_2, & c_1, & \langle 157.355, 280.805\rangle \\ & c_2, & \langle 59.2636, 60.8026\rangle \\ & c_3, & \langle -30.3249, 17.6751\rangle \end{bmatrix}$ |
| I3: Injected power harmonic | $R_3 = \begin{bmatrix} N_3, & c_1, & \langle 279.646, 342.098\rangle \\ & c_2, & \langle 59.7185, 60.3985\rangle \\ & c_3, & \langle -170.29732, 179.7027\rangle \end{bmatrix}$ |
| I4: Normal operation | $R_4 = \begin{bmatrix} N_4, & c_1, & \langle 273.315, 342.677\rangle \\ & c_2, & \langle 59.302, 60.57\rangle \\ & c_3, & \langle -34.8554, 17.8086\rangle \end{bmatrix}$ |
| I5: Islanding operation above normal operating limit | $R_5 = \begin{bmatrix} N_5, & c_1, & \langle 347.506, 3554.61\rangle \\ & c_2, & \langle 60.671, 1018.64\rangle \\ & c_3, & \langle 20.156, 180.688\rangle \end{bmatrix}$ |
| I6: Islanding operation below normal operating limit | $R_6 = \begin{bmatrix} N_6, & c_1, & \langle 0.334, 278.949\rangle \\ & c_2, & \langle 0.4, 59.34\rangle \\ & c_3, & \langle -170.29732, -32.0\rangle \end{bmatrix}$ |
| I7: Voltage flicker | $R_7 = \begin{bmatrix} N_7, & c_1, & \langle 270.19, 345.0\rangle \\ & c_2, & \langle 59.30, 64.69\rangle \\ & c_3, & \langle -174.12, 178.5\rangle \end{bmatrix}$ |

**Table 2**
Upper and lower limits of weighting and weighting centers of characteristic values.

| Category/Characteristic | $c_1$ | $c_2$ | $c_3$ |
|---|---|---|---|
| I1 (upper limit) | 572.271 | 60.4438 | 19.4 |
| I1 (center) | 455.104 | 59.8143 | −21.6 |
| I1 (lower limit) | 277.938 | 59.1848 | −31.6 |
| I2 (upper limit) | 280.805 | 60.8026 | 17.6751 |
| I2 (center) | 216.58 | 60.0331 | 1.6751 |
| I2 (lower limit) | 157.355 | 59.2636 | −30.3249 |
| I3 (upper limit) | 342.098 | 60.3985 | 179.7027 |
| I3 (center) | 311.172 | 60.1185 | −0.70268 |
| I3 (lower limit) | 279.646 | 59.7185 | −170.29732 |
| I4 (upper limit) | 342.677 | 60.57 | 17.8086 |
| I4 (center) | 311.196 | 60.127 | 0.97656 |
| I4 (lower limit) | 273.315 | 59.302 | −34.8554 |
| I5 (upper limit) | 3554.61 | 1018.64 | 180.688 |
| I5 (center) | 1002.06 | 406.36 | 98.78 |
| I5 (lower limit) | 347.506 | 60.671 | 20 |
| I6 (upper limit) | 278.949 | 59.34 | −32 |
| I6 (center) | 3.1415 | 27.9 | −60.0365 |
| I6 (lower limit) | 0.334 | 0.4 | −180.555 |
| I7 (upper limit) | 345 | 64.69 | 178.5 |
| I7 (center) | 311 | 60 | −27.99 |
| I7 (lower limit) | 270.19 | 57.3 | −174.12 |

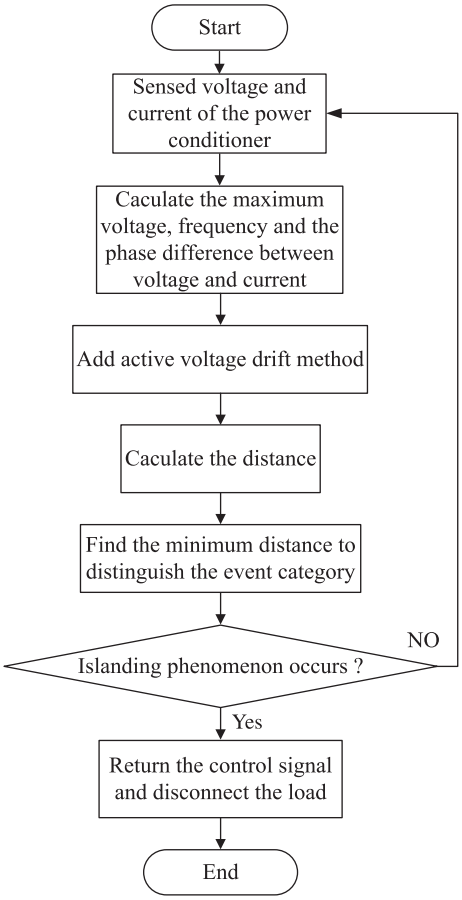


**Fig. 4.** The flowchart of the proposed extension neural network islanding detection method.

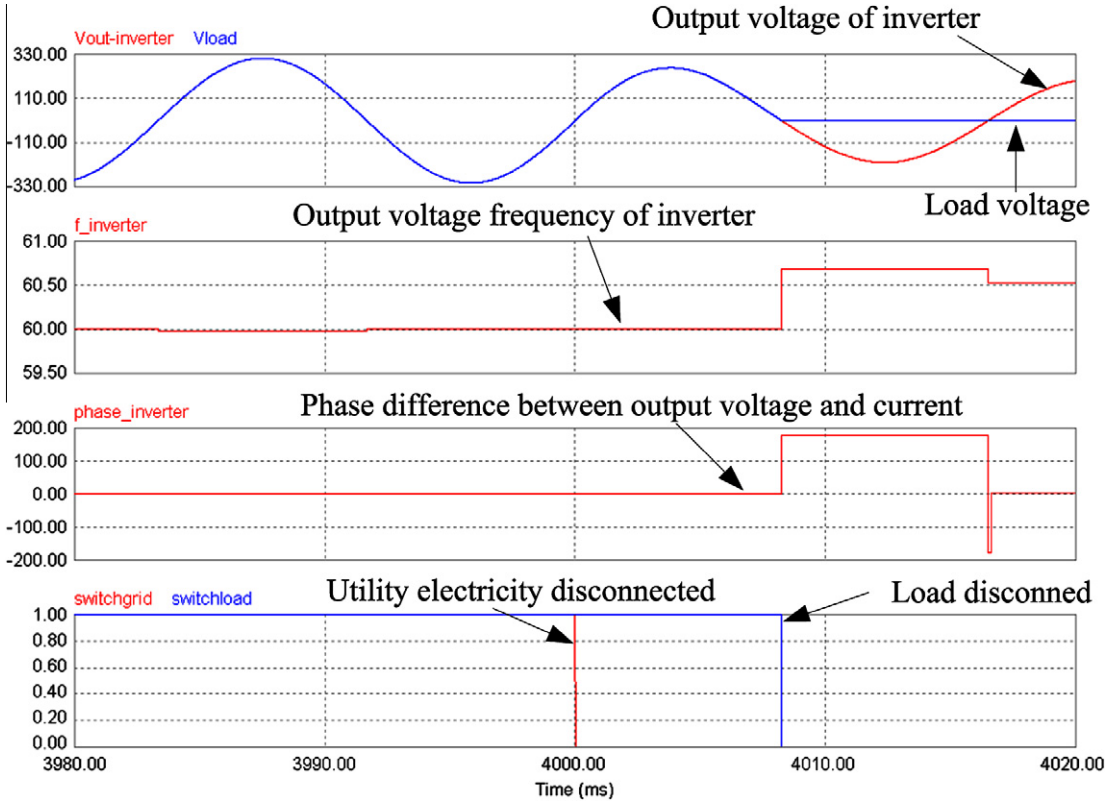


**Fig. 5.** Simulation of islanding operation detection when the grid is disconnected from system at the fourth second.

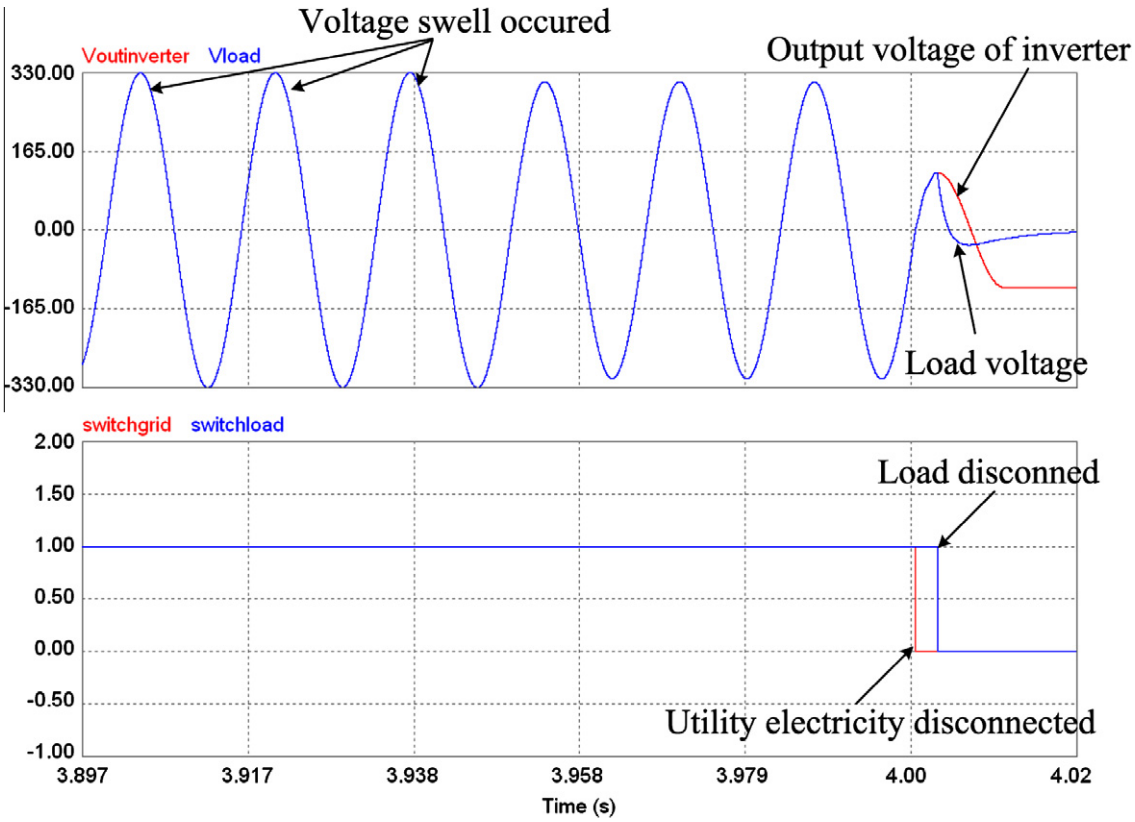


**Fig. 6.** Simulation of islanding operation detection when a voltage swell occurs.

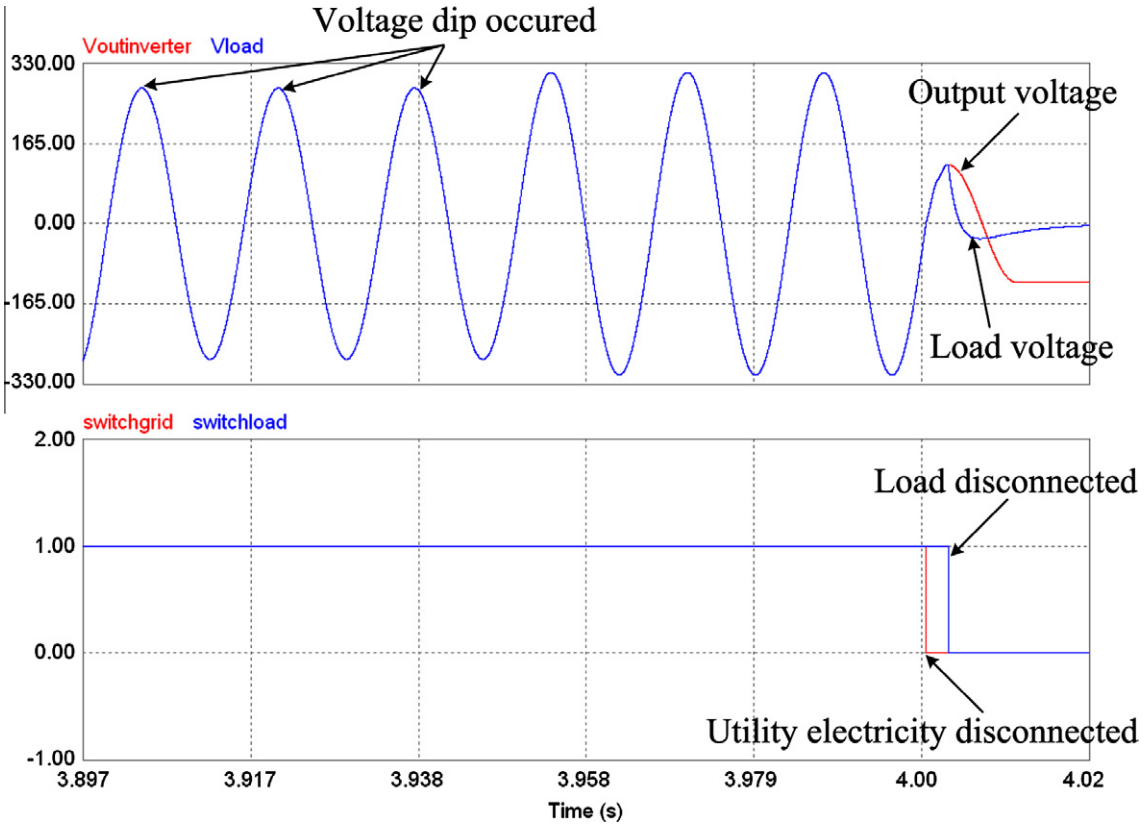


**Fig. 7.** Simulation of islanding operation detection when a voltage dip occurs.

islanding phenomenon, and the load is not cut off until the 0.5 period after the actual islanding occurrence. Fig. 7 shows the situation when a voltage dip occurs in the system, and the grid power end also has an islanding operation at about the fourth second. As seen,

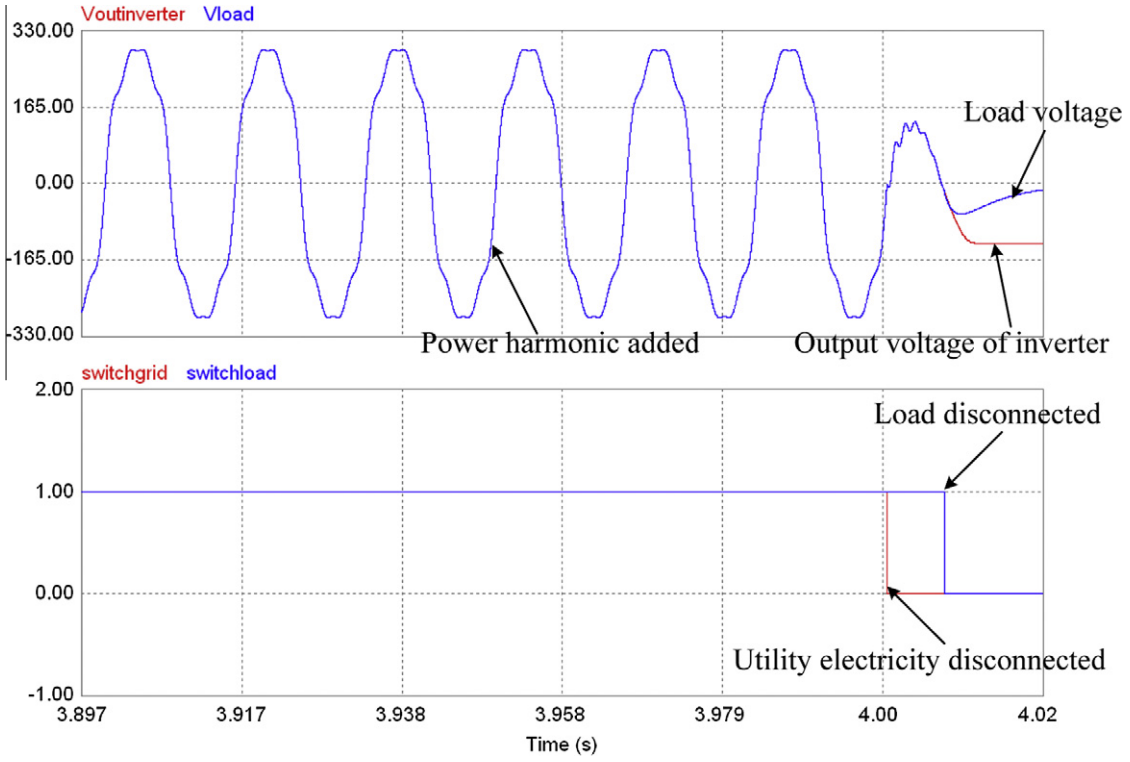


**Fig. 8.** Simulation of islanding operation detection when power harmonic occurs.

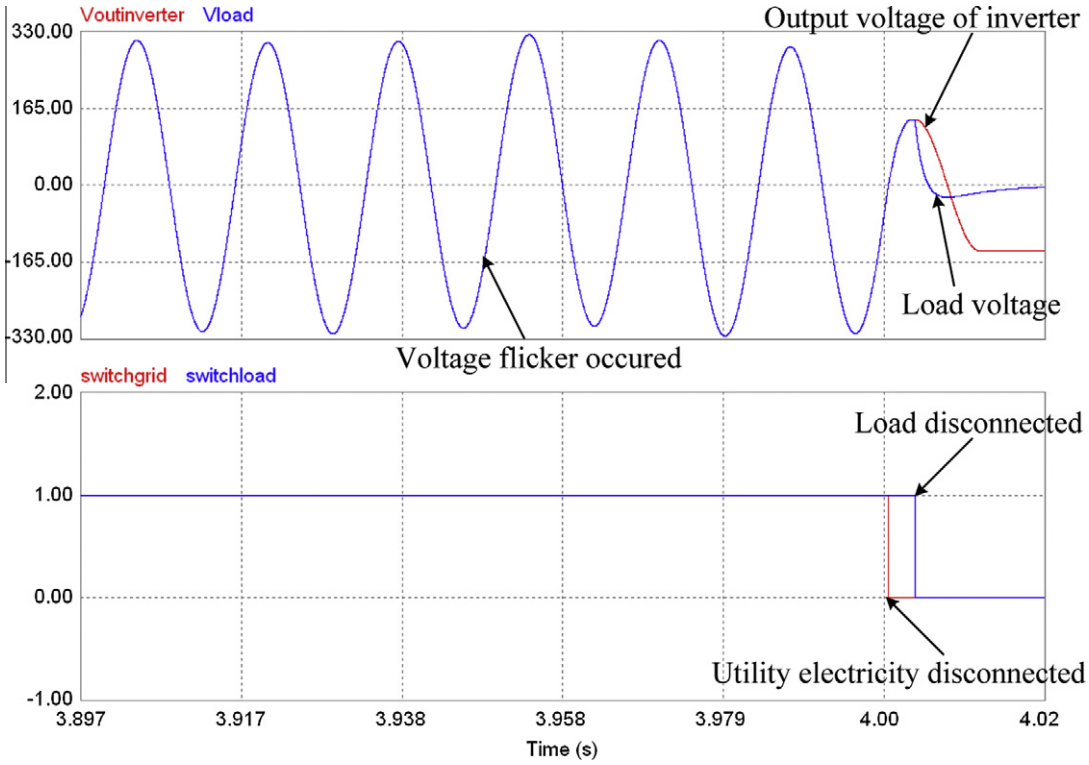


**Fig. 9.** Simulation of islanding operation detection when voltage flicker occurs.

the proposed method can definitely identify the voltage dip as electrical disturbance, and the load is cut off in a 0.5 period after the actual islanding operation.

Fig. 8 shows the simulation of an harmonic disturbance prior to an islanding operation in order to observe whether islanding detection is influenced, the harmonic components added in are the third, fifth, and seventh harmonics, and the harmonic components are 10%, 7%, and 5%, respectively, of fundamental frequency. As shown in Fig. 8, the system has an islanding operation at about fourth second, and the proposed ENN islanding detection method does not result in a misjudgment, although the system was disturbed by harmonics prior to the islanding operation. Fig. 9 shows the islanding operation detection when a voltage flicker occurs, which is formed by a 15 Hz and a 20 Hz flicker voltage and a 60 Hz standard voltage, and the actual islanding operation occurs at about the fourth second, the controller cut off the load in the 0.5 period later on islanding operation.

## 5. Conclusions

This study used an extension neural network for islanding phenomenon detection of a photovoltaic power generation system. The extension neural network theory is realized by combining the multi-variable detection methods of passive and active islanding phenomenon detections. Power quality disturbances, such as voltage swells, voltage dips, power harmonics, and voltage flickers at the grid power end are also analyzed to identify whether the abnormity at the grid power end is a power quality disturbance or an actual islanding operation. The mentioned extension neural network islanding detection algorithm is written in dynamic-link library (DLL) modules, and composed and translated by C language supported by PSIM software package. The signals sent from DLL are sent back to the controller to complete control of islanding detection. Finally, the simulation results showed that the islanding phenomenon detection method could detect islanding operations correctly and promptly cut the load from the photovoltaic power generation system within the set time.

## Acknowledgement

The authors would like to thank the Green Energy & Environment Research Laboratories, Industrial Technology Research Institute, Taiwan for financially supporting this research.

## References

Chao, K. H., Li, C. J., & Wang, M. H. (2009). A maximum power point tracking method based on extension neural network for PV systems. In *Proceedings of the 6th international symposium on neural networks on advances in neural networks*.

Hung, G. K., Chang, C. C., & Chen, C. L. (2003). Automatic phase-shift method for islanding detection of grid-connected photovoltaic inverters. *IEEE Transactions on Energy Conversion, 18*, 169–173.

IEEE Std. 1159-1995 (1995). IEEE recommended practice for monitoring electric power quality.

IEEE Std. 1547 (2003). IEEE standard for interconnecting distributed resources with electric power systems.

Jeraputra, C., & Enjeti, P. N. (2004). Development of a robust anti-islanding algorithm for utility interconnection of distributed fuel cell powered generation. *IEEE Transactions on Power Electronics, 19*, 1163–1170.

John, V., Ye, Z., & Kolwalkar, A. (2004). Investigation of anti-islanding protection of power converter based distributed generators using frequency domain analysis. *IEEE Transactions on Power Electronics, 19*, 1177–1183.

Jones, R. A., Sims, T. R., & Imece, A. F. (1990). Investigation of potential island of self commutated static power converter in photovoltaic systems. *IEEE Transactions on Energy Conversion, 5*, 624–631.

Kyocera solar industries. Kyocera photovoltaic module KC40T specifications.

Mango, F. D., Liserre, M., Aquila, & A. D. (2006). Overview of anti-islanding algorithms for PV systems. Part II: Active methods. In *Proceedings of the 12th international power electronics and motion control conference*.

Mango, F. D., Liserre, M., & Aquila, A. D. (2006). Overview of anti-islanding algorithms for PV systems. Part I: Passive methods. In *Proceedings of the 12th international power electronics and motion control conference*.

Powersim Inc. (2001–2003). PSIM User's Guide.

Sandia National Laboratories SAND 2000-1939 (2000). Development and testing of an approach to anti-islanding in utility-interconnected photovoltaic system.
Task, V. (2002). Probability of islanding in grid networks due to grid-connected photovoltaic power systems. Technical Report IEA-PVPS T5-07, p. 11.
Taiwan Power Company. Power Quality, <http://www.taipower.com.tw/>.
Wang, M. H. (2003). Extension neural network for power transformer incipient fault diagnosis. *IET Generation, Transmission and Distribution, 150*, 679–685.
Ye, Z., Li, L., Garces, L., Wang, C., Zhang, R., Dame, M., Walling, R., & Miller, N. (2004). A new family of active anti-islanding schemes based on dq implementation for grid-connected inverters. In *Proceedings of the 35th annual IEEE power electronics specialists conference*.
Ye, Z., Kolwalkar, A., Zhang, Y., Du, P., & Walling, R. (2004). Evaluation of anti-islanding schemes based on nondetection zone concept. *IEEE Transactions on Power Electronics, 19*, 1171–1176.